Poster Abstracts: Clinical MRI—Vascular Disease

294. Prognosis of Aortic Dissection Submitted to Surgery. Influence of Aortic Mechanical Function Assessed by Magnetic Resonance Imaging

Ana G. Almeida, MD, PhD,[1] Miguel Pacheco, MD,[1] Joao Fancony, MD,[2] Luis Beija, MD,[2] Joao Cravino, MD,[2] M-Celeste Vagueiro, MD.[2] [1]*Cardiology, University Hospital Santa Maria, Lisbon, Portugal,* [2]*Cardiothoracic Surgery, University Hospital Santa Maria, Lisbon, Portugal.*

Introduction: Aortic mechanical function was an independent predictor of aortic dilatation in Marfan. Patients (pts) operated for aortic dissection remain at risk of late complications, namely aneurysm and rupture of the residual aorta.

Purpose: The aim of this study was to assess the prognostic influence of aortic mechanical function indexes, evaluated by magnetic resonance (MR) on the late evolution of operated aortic dissection.

Methods: We studied 47 consecutive pts operated for type A aortic dissection (ascending aorta graft in all pts, aortic valve re-suspension in 16 and aortic valve prosthesis in 14), 26 men, aged 53.8 ± 11.1 years old. All were submitted to magnetic resonance imaging (MRI) two months after surgery and afterwards, annually, for three years. MR study: GE Signa 1.5T; high resolution spin-echo and cine MR. For analysis, residual aorta was divided in 3 segments: 1-arch; 2-descending thoracic; 3-abdominal. In order to assess long-term evolution, we evaluated segments dimensions and presence of residual flap, at initial and follow-up studies. Mechanical function indexes were obtained at the initial evaluation: 1. Pulse pressure (mmHg); 2: Segmental indexes—area strain; distensibility (dynes/cm^2); elastic modulus (dynes/cm$^2 - 1$); beta stiffness index. Aortic aneurysm were considered when the dimension of a thoracic segment was >49 mm and abdominal >39 mm.

Results: Mean follow-up was 39.5 ± 0.56 months. No patient had aneurysm on early evaluation. A group of 23 pts had a residual flap. Complications detected: aneurysm development in 35 segments, from 22 pts. Mechanical function influence: 1. Pts with aneurysm in any segment had higher pulse pressure than pts without aneurysm (57.8 ± 4.4 vs 41.6 ± 3.8, p = 0.000); 2. Pts with aneurysm in segment 1 had lower strain (7.4 ± 1.7 vs 19.1 ± 1.7, p = 0.000), lower distensibility (0.35 ± 0.11 vs 0.83 ± 0.08, p = 0.000) and higher beta stiffness index (0.9 ± 0.3 vs 0.5 ± 0.1, p = 0.003); 3. Pts with aneurysm in segment 2 had lower strain (11.6 ± 1.7 vs 23.6 ± 1.1, p = 0.000), lower distensibility (0.47 ± 0.08 vs 1.25 ± 0.11, p = 0.005), higher elastic modulus (5.6 ± 0.8 vs 2.6 ± 0.2, p = 0.004) and higher beta stiffness index (0.71 ± 0.08 vs 0.35 ± 0.05, p = 0.000); 4. There was no association between the development of aneurysm in segment 3 and mechanical indexes. 5. In the subgroup of pts without a residual flap (25 pts) there was a more significant difference between mechanical indexes of segments with and without aneurysms.

Conclusion: Pts operated for aortic dissection had a high incidence of late aneurysm development. This complication was associated with indexes of higher aortic stiffness at early evaluation. This knowledge may influence the follow-up strategy of this aorthopaty.

295. 2D Spatially-Selective RF Excitation for Real-Time High-Resolution Phase Contrast MR Imaging: Quantification of Hyperemic Flow in the Femoral Artery

Juerg Schwitter, MD,[1] Markus Oelhafen, MSE,[2] Barbara M. Wyss, MD,[1] Armin Kraus,[1] Beatrice Amann, MD,[3] Thomas F. Luescher, MD,[1] Peter Boesiger, PhD.[2] [1]*Division of Cardiology, University Hospital Zurich,*

Zurich, Switzerland, [2]Institute of Biomedical Engineering and Medical Informatics, Federal Institute of Technology ETH, Zurich, Switzerland, [3]Division of Angiology, University Hospital Zurich, Zurich, Switzerland.

Background: To study vascular function at a predilection site of atherosclerosis would be highly desirable. Aim: To develop a real-time high-resolution phase-contrast MR technique (rtPC-MR) for monitoring ischemia-induced hyperemic flow (hF) in the femoral artery.

*Methods:* Thirteen age-matched healthy volunteers and 17 patients; mean age 49 ± 6 years) with cardiovascular risk factors but without stenoses in the femoral arteries were studied with rtPC-MR. A 2D spatially-selective radiofrequency pulse yields a spatial and temporal resolution of $1 \times 1mm^2$ and 48ms, respectively (Fig. 1). Conventional retrospectively-gated phase-contrast MR (refMR, spatial/temporal resolution $1 \times 1mm^2/22ms$, acquisition duration 6 min) was used for reference and was immediately preceded and followed by a rtPC-MR measurement over 49 seconds. Resting measurements were repeated once and were followed by induction of ischemia in the lower leg by means of a 4-minute cuff occlusion. hF was measured following cuff release. Ischemia induction and
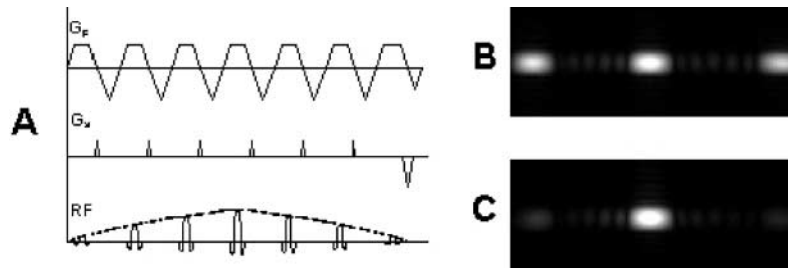
Figure 1. 1A: 2D spatially selective rf pulse with 2 gradients (Gp and Gs) for spatial selection. 1B: Resulting 2D selective excitation. 1C: The central excitation profile is selected by the surface coil.
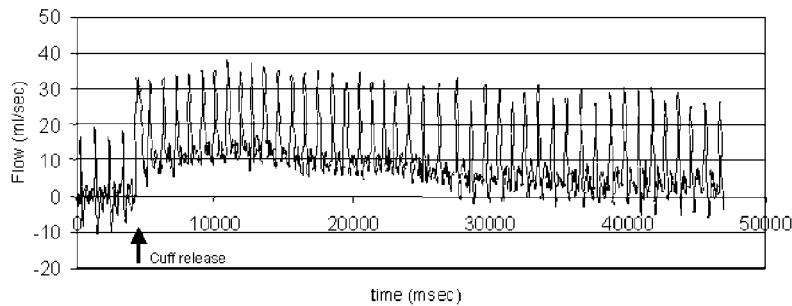

Figure 2. Representative hyperemic flow curve in a healthy volunteer. Vacuum-driven release of cuff causes immediate increase in flow.
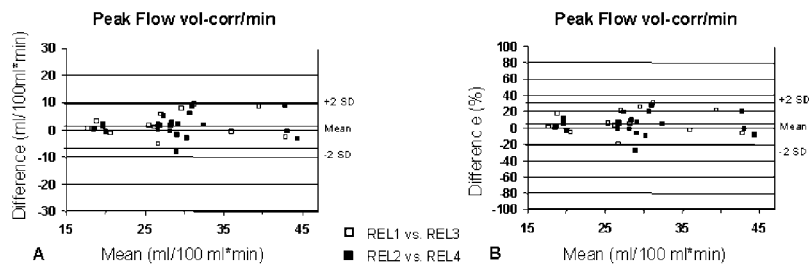
Figure 3. Agreement of resting flow measurements by rtPC-MR and refMR is high and matches reproducibility of the two techniques (see Table 1).

MARCEL DEKKER, INC. • 270 MADISON AVENUE • NEW YORK, NY 10016

Table 1.

| | Resting flow (n = 88) mL/beat | Reproducibility (88 measurements; mean ± SD) (mean interval: 9 ± 12 days) | | | | | |
| | | Resting flow | | Peak hF | | Area under hF curve | |
		mL/beat	%	mL/min/100mL	%	mL/100mL	%
rtPC-MR	3.25 ± 1.29	0.20 ± 0.37	5.9 ± 12.1	1.5 ± 4.0	5.1 ± 13.0	0.29 ± 1.76	3.2 ± 16.5
refMR	3.23 ± 1.39	0.21 ± 0.38	6.1 ± 12.2	—	—	—	—

Comparison rtPC-MR vs refMR: Resting flow in femoral artery
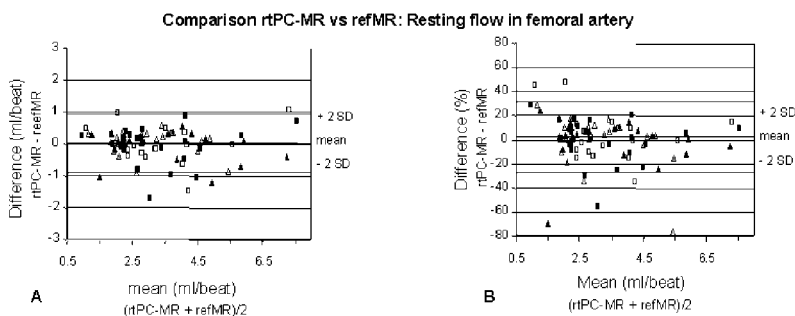
Figure 4. Reproducibility for peak hyperemic flow per minute (at a heart rate of 60 bpm) for 100mL of lower leg volume is high.

hF measurement was also repeated once. At a mean of 9 ± 12 days the entire protocol was repeated in 24 subjects (12 volunteers, 12 patients). A representative hyperemic flow curve is shown in Fig. 2.

Results: Agreement between rtPC-MR/refMR was −2.5 ± 14.5% (mean difference ± SD, see also Fig. 3) with a similar reproducibility for both techniques (Table 1 and Fig. 4). hF in patients (with 1.9 ± 1.1 ATPIII risk factors) was reduced vs controls (0.41 ± 0.005 mL/beat/100mL of lower leg volume versus 0.50 ± 0.015mL/beat/100mL, respectively, p = 0.011) and correlated inversely with the number of risk factors (r = −0.46, p < 0.011). Area under the response curve was not different for controls and patients.

Conclusions: This rtPC-MR technique for the first time allows measurement of ischemia-induced hyperemic flow in the lower leg. Due to its high precision and reproducibility, this technique is ideal to study vascular function at a predilection site for atherosclerosis.

296. Vessel Wall Area Measurement in the Atherosclerotic Carotid Artery: Reproducibility Assessment Using High Resolution MR Imaging with Multi-contrast Weightings

Shao-xiong Zhang, M.D./PhD,[1] Claudia Hillenbrand, PhD,[1] Yiping Chen, M.D./PhD,[2] Frank K. Wacker, M.D.,[1] Jeffrey L. Duerk, PhD,[1] Jonathan S. Lewin, M.D.[1] [1]*Radiology-MRI, University Hospitals of Cleveland, Case Western Reserve University, Cleveland, OH, USA,* [2]*Cardiology, University Hospitals of Cleveland, Case Western Reserve University, Cleveland, OH, USA.*

Introduction: Black blood high resolution MRI techniques with multiple contrast weightings have been shown to be useful for atherosclerotic tissue characterization and for plaque area measurement which is known to represent a direct measure of plaque burden. This allows reliable monitoring of regression and progression of atherosclerosis. Hence, it is widely accepted that an ideal MRI protocol for atherosclerotic plaque characterization and quantification should include multi-contrast weightings. However, to measure plaque area in all available images from all sequences is very time consuming. Measuring it from one set of contrast-weighted images would be more clinical practicable. Unfortunately, it is, unclear whether carotid plaque burden measurement from the three most commonly used contrast weightings will provide similar results.

Purpose: This study was performed to test the hypothesis that wall area measurements from three different contrast-weightings (T1W, T2W and PDW) acquired at the same time yield similar results. In addition the intra-observer variability or reproducibility of the carotid wall area measurements was tested.

Methods: Eight patients (aged 72 ± 7 years) with carotid stenosis documented by duplex ultrasound were recruited for the study. Informed consent was obtained under a protocol approved by the institutional review board for human investigation.

All MR scans were conducted on a 1.5 T scanner (Magnetom Sonata. Siemens Medical Solutions, Germany) with a custom-built phased array coil which was used to improve the signal-to-noise of the images. A 3-dimensional (3D) multiple overlapping thin slab angiography (MOTSA) sequence with TR/TE/flip angle/partition thickness $= 20\,\mathrm{ms}/3.4\,\mathrm{ms}/25°/1.0\,\mathrm{mm}$, was used to locate the exact level of the carotid bifurcation. Dark blood images were then obtained using an ECG-triggered double inversion recovery (DIR) turbo spin echo sequence. The imaging parameters (TR/TE/TI/NEX/thickness/FOV) were as follows: T1W: 1R-R/7.1ms/500ms/2/3mm/13cm; PDW: 2R-R/7.1ms/600ms/2/3mm/13cm; T2W: 2R-R/68ms/600ms/2/3mm/13cm. The in plane resolution is $0.51 \times 0.51\,\mathrm{mm}^2$.

The carotid lumen and outer wall boundaries were manually segmented on a freestanding image processing station (MR View, Siemens, Erlangen, Germany). The outer vessel wall boundary was defined as the vessel wall-perivascular soft tissue interface. The wall area was defined as the area calculated by subtracting the lumen area from the outer wall boundary area. Maximum wall area (MaxWA) was defined as the largest area measured from the distal common carotid, the bifurcation, and the internal carotid artery wall. Segmentation of the lumen and outer wall boundary was performed on each image set independently by trained physicians who were also blinded to the measurement results obtained on other image contrast weighted data sets. Measurement of each image data set was repeated at a different time by the same observer, again blinded from all other measurements. The average time between measurements was 10 days. The measurement data was imported to Excel 2000 for statistical analysis. Mean differences of carotid wall area and MaxWA of inter-contrast weighting and intra-rater variability were calculated and assessed by paired Student's t-test. A value of $p < 0.05$ was considered significant.

Results: The average scan time was 40 minutes (including set up time) and all subjects tolerated the scan without complaints or complications. Three different contrast weightings, T1, T2 and PD, were successfully acquired in all subjects with satisfactory flow signal suppression. Seventy-six images of each contrast weighting from matched location from 8 patients were available for this study.

The mean carotid wall area for T1W, PDW and T2W images was $54.0\,\mathrm{mm}^2$, $53.0\,\mathrm{mm}^2$ and $51.0\,\mathrm{mm}^2$ respectively with difference of $PD - T1$, $T1 - T2$ and $PD - T2$ as $0.0 \pm 8.0\,\mathrm{mm}^2$ ($P = 0.37$), $3.0 \pm 8.0\,\mathrm{mm}^2$ ($P = 0.002$) and $3.0 \pm 8.0\,\mathrm{mm}^2$ ($P = 0.002$) respectively.

The mean carotid MaxWA for T1W, PDW and T2W images was $84.4\,\mathrm{mm}^2$, $84.4\,\mathrm{mm}^2$ and $75.0\,\mathrm{mm}^2$ respectively with difference of $PD - T1$, $T1 - T2$ and $PD - T2$ as $0.3 \pm 0.1\,\mathrm{mm}^2$ ($P = 0.94$), $9.9 \pm 12.2\,\mathrm{mm}^2$ ($P = 0.08$) and $9.9 \pm 7.7\,\mathrm{mm}^2$ ($P = 0.007$) respectively. No statistically significant difference was noted for the intra-rater measurements. The difference of carotid wall area for T1W, PDW and T2W images was $4.2 \pm 6.1\mathrm{mm}^2$ ($P = 0.229$), $5.5 \pm 4.3\,\mathrm{mm}^2$ ($P = 0.52$) and $5.5 \pm 5.2\mathrm{mm}^2$ ($P = 0.056$) respectively. The intra-rater difference of carotid MaxWA for T1W, PDW and T2W images was $5.5 \pm 2.5\,\mathrm{mm}^2$ ($P = 0.899$), $8.0 \pm 4.0\,\mathrm{mm}^2$ ($P = 0.772$) and $9.8 \pm 11.1\,\mathrm{mm}^2$ ($P = 0.226$) respectively.

Conclusions: The carotid wall area measurements from T1W and PDW images, were comparable in this study with a low intra-rater variability on repeated measurements. This suggests that both weightings can be used interchangeably for monitoring plaque burden regression and progression. This is in accordance with recent reports which showed highly accurate in vivo measurement of artery wall areas in atherosclerotic carotid lesions with T1W and PDW methods. T2-weighted images provided smaller carotid wall area values, although it has similar intra-rater reproducibility as T1W and PDW images. Hence, use of this image contrast for calculation of wall area has the potential to underestimate the plaque burden. Our results suggest that T1W and PDW images are best suited for plaque burden evaluation. Due to their interchangeability, only one set of images is needed for the vessel wall area measurement, which is more practicable in a routine clinical setup.

297. 3D MR Angiography Overestimates Pulmonary Vein Diameter as Compared to 2D Cine MRI

Mushabbar Syed, MD, Dana Peters, Ph.D, Andrew Arai, MD. *Laboratory of Cardiac Energetics, National Heart, Lung & Blood Institute, Bethesda, MD, USA.*

Introduction: Paroxysmal atrial fibrillation (PAF) has been associated with focal triggers located near or around pulmonary vein (PV) orifices. This information has led to development of catheter based interventions to ablate these foci. PV imaging is an important component of

catheter based therapy for PAF. Identification of all PV orifices is not only an integral part of the electrophysiological mapping and ablation of atrial fibrillation foci but is also important in the assessment of post-ablation PV ostial stenosis. Newly developed balloon tipped catheters which fit in the PV orifice to aid with ablation procedure are under investigation. This requires an assessment of PV orifice size for adequate catheter fit. Currently, PV imaging for this procedure is being done either with 3D-high resolution computed tomography or pulmonary angiography. Magnetic resonance imaging (MRI) has the advantage of a non-invasive imaging modality with excellent resolution and does not require administration of iodinated contrast medium. Initial studies evaluating 3D MR angiography (3D-MRA) of PV have reported excellent anatomical characterization. We are developing MRI methods suitable for characterizing pulmonary vein anatomy, orifices and orifice size that might facilitate catheter ablation of PV foci.

Purpose: We hypothesized that cardiac motion might degrade the ability to quantify pulmonary vein size on standard contrast enhanced 3D-MRA.

Methods: Patient selection: For PV imaging experiments we used nine normal adult volunteers with normal sinus rhythm.

Pulmonary vein imaging: PV anatomy, size, and blurriness was assessed on 2D cine MRI and non-gated 3D-MRA. Imaging was performed on clinical 1.5 T scanner (GE Medical Systems, USA). To provide high resolution images of PV size and motion across the cardiac cycle, 2-D multi-phase segmented ECG-gated axial slices were obtained using steady state free precession (**2D-SSFP**) in multiple breath-holds. Imaging parameters were: 192×192, 32 to 36 cm FOV, 3/4 fractional FOV, full echo, $+/- 125$ kHz bandwidth, 5 mm slices, TR/flip = 3.1 ms/50 degrees, 12 views per segment, 14 second breath-hold. This provided acquisition window of 37 ms, and $1.9 \times 1.9 \times 5$ mm spatial resolution.

Coronal **3D-MRA** was performed by scanning during peak arterial enhancement after injection of 0.1 mmol/kg of gadolinium contrast agent at 1 ml/s, followed by a saline flush. Imaging parameters were: 512×192 to 160 phase-encodings, 32 to 36 cm FOV, 0.8 fractional FOV, 20 to 24 slices, 3.6 mm thick before zero filling, fractional echo, ± 62.5 kHz bandwidth, TR/flip = 6.2 ms/45 degrees, 20 second breath-hold. Images were mask subtracted and then reformatted into the axial plane. Axial slices which contained views of the pulmonary vein corresponding to the 2D-SSFP images were analyzed. The spatial resolution in the axial plane was 2.7×3.6 mm (prior to zero filling).

Measurements of PV diameters: PV diameters were measured at the orifice (junction of PV and left atrium) and at another site, 1 cm proximal to the orifice. Measurements were obtained on axial cine MRI images and on corresponding axial reformatted 3D-MRA images. 3D-MRA allowed only one measurement across the cardiac cycle. The maximum and minimum PV diameter across the cardiac cycle was measured at both sites (orifice and 1cm proximal to orifice) and averaged on all PV visualized with 2D-SSFP. For both 3D-MRA and 2D-SSFP, each pulmonary vein was assigned a Blurriness Score (0-4) depending on the sharpness of borders and orifices, as follows: $0 = $ non$-$diagnostic, $1 = $ poor, $2 = $ fair, $3 = $ good and $4 = $ excellent.

Statistical Analysis: Measurements were compared with a two-tailed paired t-test. Blurriness score was compared with a Mann Whitney rank order test. Results are reported as mean $+/-$ standard deviation.

Results: Mean age of the volunteers was 41.7 ± 11.1 years and mean heart rate was 72 ± 6.5 beats/min. All PV were identified by 2D-SSFP and 3D-MRA except for a left superior PV in one subject missed by 2D-SSFP and one non-diagnostic 3D-MRA due to bolus timing error. Qualitatively, 3D-MRA provided graphically impressive image quality (Fig. 1).

However, 3D-MRA overestimated minimum, average, and maximum PV diameters compared with 2D-SSFP (Table 1 when grouping all 4 pulmonary veins per subject). In subgroup analysis by individual PV, 3D-MRA overestimated average PV diameter. These differences were statistically significant for all except left superior PV on ostial measurements but only for right inferior PV on measurements taken 1 cm from the ostium due to sample size limitation. The blurriness score was worse for all four PV for 3D images as compared to 2D-SSFP. Blurriness scores for 3D-MRA as compared to 2D-SSFP imaging were as follows: left superior PV 1.2 ± 1.1 vs. 2.6 ± 1.1 (p = 0.04), right superior PV 1.2 ± 0.7 vs. 3.4 ± 0.7 (p < 0.001), left inferior PV 1.6 ± 0.9 vs. 4 ± 0 (p < 0.001) and right inferior PV 2.1 ± 1.3 vs. 3.8 ± 0.7 (p = 0.003).

Figure 1. A subtracted 2D slice from 3D-MRA showing 4 pulmonary veins & left atrium (LA).

Table 1. Comparison of PV measurements on 3D-MRA and 2D-SSFP.

PV Diameter (mm)	Ostial	1 cm from Ostium
3D-MRA	14.6 ± 2.8	14.5 ± 3.4
2D-SSFP (average)	11.4 ± 2.3***	11.9 ± 1.9***
2D-SSFP (minimum)	10.2 ± 2.6***	11.1 ± 2.1***
2D-SSFP (maximum)	12.6 ± 2.1***	12.9 ± 1.9*

Statistics: * = $p < 0.05$, *** = $p < 0.001$.

Conclusion: While 3D-MRA produces excellent anatomic depictions of the pulmonary veins, these images overestimate pulmonary vein size compared to gated studies. This overestimation is likely due to movement of PV across the cardiac cycle in addition to phasic changes, causing blurring of PV margins and ostium on 3D-MRA images. PV dimensions were easily measurable by 2D cine MRI with clear delineation of margins and orifices.

298. Measurement of Skeletal Muscle Perfusion in Normal Volunteers During Reactive Hyperemia: Validation of Gadolinium Enhanced Methods Using MR Plethysmography and Arterial Blood Flow Techniques

Richard B. Thompson,[1] Venkatesh K. Raman,[1] Alexander J. Dick,[1] Guy Shechter,[2] Robert S. Balaban,[1] Elliot R. McVeigh,[1] Robert J. Lederman.[1] [1]*National Heart Lung and Blood Institute, National Institutes of Health, Bethesda, MD, USA,* [2]*Department of Biomedical Engineering, Johns Hopkins University School of Medicine, Baltimore, MD, USA.*

Introduction: Obstructive peripheral artery disease affects 15% of adults over age 55, of whom over one-third are symptomatic. Typical manifestations are pain during walking or threat of limb loss. Lower extremity perfusion measures would be useful in the development of novel biological treatments. However, no robust global or regional measurements are available. Measurement of circumferential muscle swelling with venous occlusion strain-gauge plethysmography (SG-P), the prevailing standard for non-invasive measurement of limb perfusion, is limited by significant systematic underestimation of flow (Saltin B, Am. J. Cardiol. 62: 30E–35E (1988)). SG-P also provides only global as opposed to regional flow information. Finally, lower extremity perfusion measures are best obtained during post-ischemic reactive hyperemia (RH), which is less susceptible to fluctuations in vascular tone than resting blood flow measurements. The short duration of RH (peak flows typically lasting several seconds) imposes demands on the temporal resolution of MR-based perfusion measures. We present here an investigation of several lower-extremity perfusion measures that might serve as attractive tools for diagnosis and assessment of response to treatment, such as investigational therapeutic angiogenesis.

Purpose: We validate blood flow in skeletal muscle during reactive hyperemia (RH) measured by gadolinium (Gd-DTPA) inflow-enhanced MR with MR plethysmography (MR-P) and real-time phase-contrast (PC) MRI.

Methods: In four normal volunteers, post-ischemic RH in the calf was induced by 5 minutes of thigh-cuff inflation to supersystolic pressures (180–220 mmHg) to occlude arterial inflow. Immediately following arterial cuff deflation, a second thigh-cuff was inflated to occlude venous outflow (40 mmHg). Both cuffs were inflated/deflated using an automated plethysmography system (D.E. Hokanson, Bellevue, WA). MR imaging was performed on a Siemens 1.5 T Sonata scanner (Siemens Medical Sytems, Erlangen, Germany) using a standard head coil. A series of two post-ischemic RH experiments were used with each volunteer for comparison of flow measurement techniques. In the first, PC-MRI was used to measure bulk blood flow in the popliteal artery during the hyperemic flow period. Following a 15 minute recovery period, the flow response to RH was measured with interleaved saturation recovery Gd-DTPA (Magnevist, Berlex, Wayne, NJ) inflow and MR-plethysmography high spatial resolution anatomical imaging experiments. Due to the transient nature of RH, the bulk blood flow was measured with a real-time PC-MRI pulse sequence, targeting flow in the popliteal artery at the level of the knee. The Gd-DTPA saturation recovery (Ti = 160 ms) and MR-P exams were both FISP pulse sequences: FOV = 24 × 19 cm, slice thickness = 10 mm, flip angle = 60 degrees, TR = 5.0 ms/3.4 ms, TE = 2.5 ms/1.7 ms, BW = 20 kHz /150 kHz, matrix = 64 × 64/192 × 154, respectively.

The interleaved experiments were run continuously for 2 minutes beginning 20 seconds prior to the arterial cuff release, with a temporal resolution of 890 ms for both acquisitions. One minute after arterial cuff inflation, the Gd-DTPA (0.1mmol/kg) was injected to allow contrast equilibration in the blood pool. Arterial cuff release (with simultaneous venous cuff inflation) begins a square-wave input of contrast agent concentration in the arterial blood and concurrent swelling of the calf. An ankle cuff was inflated to 200mmHg prior to all arterial cuff inflations to exclude pedal flow from the measured hyperemic response.

PC-MRI flow data was normalized for muscle mass estimated from three-dimensional calf images. Gd-DTPA flow was calculated using the mean transit time (MTT), calculated directly from the inflow enhanced data, assuming a distribution volume (extracellular volume) in skeletal muscle of 0.08 (Donahue KM et. al., MRM 34: 423–432 (1995)) ($F = $Volume/MTT). The MTT was calculated using the impulse response, which is the time-derivative of the inflow signal intensity curve (Fig. 1a). MR-P cross sectional areas were automatically calculated using B-spline snakes that tracked the outer fat boundary in time, without user interaction. Partial volume (PV) correction for fat and bone was done for all volunteers. MR-P data was also processed with an assumption of 3D-isotropic growth rather than 2D-planar growth (factor = 1.5). All data analysis was done using MATLAB (Mathworks, Natick, MA).

Results: Examples of raw measured flow data, for volunteer 3, is shown in Fig. 1. Figure 1a displays a sample gadolinium inflow signal intensity curve and the corresponding calculated impulse response for a $20\,cm^2$ ROI from the gastrocnemius muscle. The flow rate for this sample ROI is $F = 0.08/(6.6\,sec/60\,sec/min) = 73\,mL/100\,mL$ muscle/-min. The PC-MRI flow curve is shown in Fig. 1b, where the peak flow rate is 16ml/s, corresponding to a flow rate of $16\,ml/s*60\,sec/min/1620\,ml = 59\,mL/100\,mL$ muscle/min, where 1620ml is the measured muscle volume. Figure 1c displays the percentage change in calf cross-sectional area over time, with a peak rate of 27mL/100mL muscle/min. Multiple venous cuff inflations/deflations, shown in Fig. 1c, allow the recovery from hyperemia over time to be measured (not reported here). Figure 2 displays the RH blood flow measured with the three methods in each of the four volunteers. The Gd-DTPA flow values are averaged for the entire muscle mass, although S/N is sufficiently high (>100) to allow single voxel (.14 ml) flow analysis. MR-P values are shown; i) as measured directly, ii) with a correction
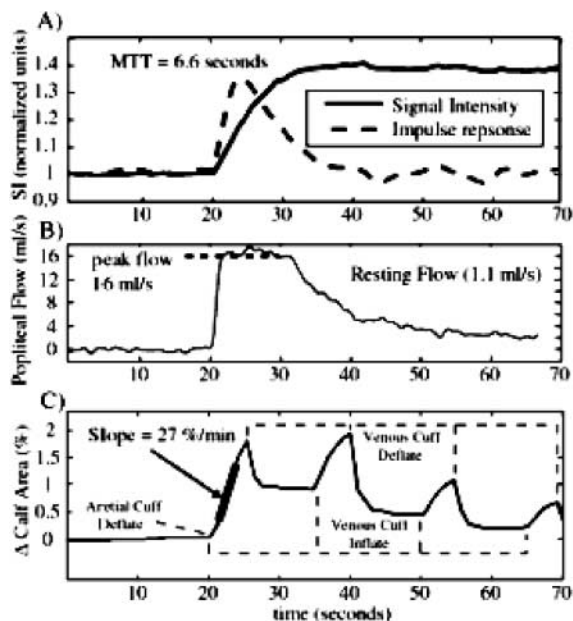

Figure 1.

for partial volume effects, and iii) for an assumption of isotropic swelling.

Conclusions: Skeletal muscle blood flow measured with gadolinium inflow-enhanced MRI during reactive hyperemia agrees with bulk flow values measured with real-time phase-contrast MRI. There is sufficient S/N (>100) with gadolinium inflow studies to do regional flow analysis in skeletal muscle, allowing comparison of flow between muscle groups.
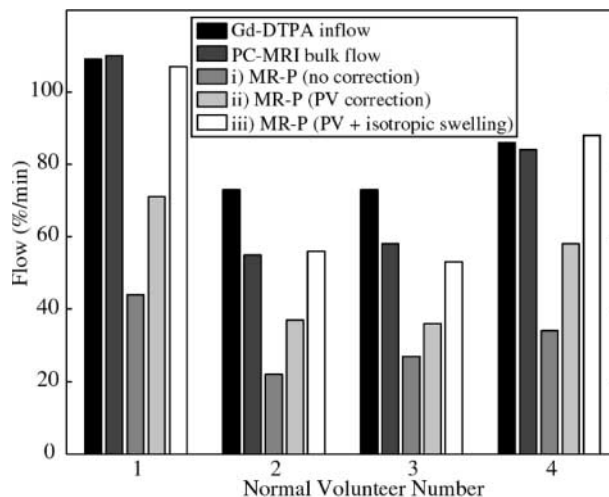

Figure 2.

Plethysmographic flow values significantly underestimate the flow as compared to the former two methods. Correction of MR- plethysmographic flow values for partial volume effects, not possible with strain-gauge plethysmography, and the assumption of 3D-isotropic growth resulted in excellent agreement with gadolinium and bulk flow measures.

299. Coronary Artery Imaging Using 3D Breath-Hold True-FISP with 2D Iterative Partial Fourier Reconstruction

Ravi K. Singh, MS,[1] Vibhas S. Deshpande, MS,[1] Steven M. Shea, MS,[1] E. Mark Haacke, PhD,[2] Richard M. McCarthy, MD,[1] James Carr, MD,[1] Debiao Li, PhD.[1]
[1]Department of Radiology, Northwestern University, Chicago, IL, USA, [2]Magnetic Resonance Institute for Biomedical Research, St. Louis, MO, USA.

Introduction: In magnetic resonance angiography (MRA) of the coronary arteries, the necessity for breath-hold limits imaging time which can lead to decreased spatial resolution. One method of reducing acquisition time is partial Fourier (PF) imaging which allows high resolution imaging using less k-space data. A two-dimensional (2D) projection onto convex sets (POCS) method has been successfully applied to imaging of the brain and MRA of the leg, but has not been assessed in MRA of the coronary arteries with true-FISP sequences.

Purpose: The purpose of this study is to compare the quality of images generated using a 2D PF reconstruction scheme with half of the k-space data to images reconstructed from the full k-space data set in true-FISP MR imaging of coronary arteries.

Methods: Data Acquisition: K-space raw data sets of the coronary arteries of seven volunteers were collected using a three-dimensional (3D) breath-hold true-FISP (fast imaging with steady-state precession) sequence. The imaging parameters were as follows: $TR/TE/\alpha = 3.50\,ms/1.75\,ms/70°$, $FOV = (164-226) \times 250\,mm^2$, acquisition matrix $(124-164) \times 256$, lines per segment $(31-41)$, number of partitions $6-8$, slab thickness 18 mm, breath-hold time 24 cardiac cycles. The k-space coverage was symmetric about the origin, with 128 points before and after the echo, and an equal number of lines above and below the origin. The number of lines collected was variable due to variability in the R–R interval.

Image Reconstruction: All images were reconstructed offline with MATLAB software.

A one-dimensional Fourier transform was first performed in the slice-selection direction to give partitions of 2D k-space data. Three sets of images were reconstructed. The first set was reconstructed from full k-space data, the second set from partial k-space data with a PF estimations, and the third set from partial k-space data with zero-filling.

Full k-space Images: The original data set was used to reconstruct the full k-space images.

Zero-Filled (ZF) Images: These images were reconstructed by using 75% of the data collected in the readout direction, and 75% of the data collected in the phase encoded direction and zero-filling the remaining data. In the readout direction, the first 64 points were replaced with zeroes and final 192 points were used, and in the phase direction, the first 75% of the lines were used and the final 25% were replaced with zeroes (e.g., if 160 lines were collected, lines 1–120 were used and lines 121–160 were replaced with zeroes).

PF Images: These images were reconstructed by using 75% of the data collected in the readout direction, and 75% of the data collected in the phase encoded direction and estimating the remaining data with a PF technique.

The PF method used the POCS concept which has been shown to reliably estimate the missing k-space data using a low-resolution phase map (1). A magnitude image reconstructed from the partial, asymmetric k-space data was used as the first approximation of the true magnitude image. The low resolution phase map was generated from a sampling of the center of k-space. The 64 points before and after the echo and the central 50% of the lines in the phase direction were used (e.g., if there were 160 lines collected, lines 41–120 were used). The rest of k-space was zero-filled, and a Hamming filter was applied to prevent discontinuities. The approximate magnitude image and the low resolution phase map were combined, and the data was transformed back into an estimate of the k-space data. The estimated k-space values that overlapped with the partial, asymmetric k-space data were replaced by the original k-space data, and a Hamming filter was again applied to prevent discontinuities. The magnitude image created from this data set was used as the next approximation of the true magnitude image. Five iterations of the algorithm were performed.

Image Analysis: The image quality for all seven studies was rated both quantitatively and qualitatively. Coronary artery sharpness was quantified with Scion Image software by measuring intensity profiles along user-defined lines perpendicular to the major axes of the vessels, as has been described previously (2). Coronary artery definition was also rated qualitatively on a scale of

MARCEL DEKKER, INC. • 270 MADISON AVENUE • NEW YORK, NY 10016
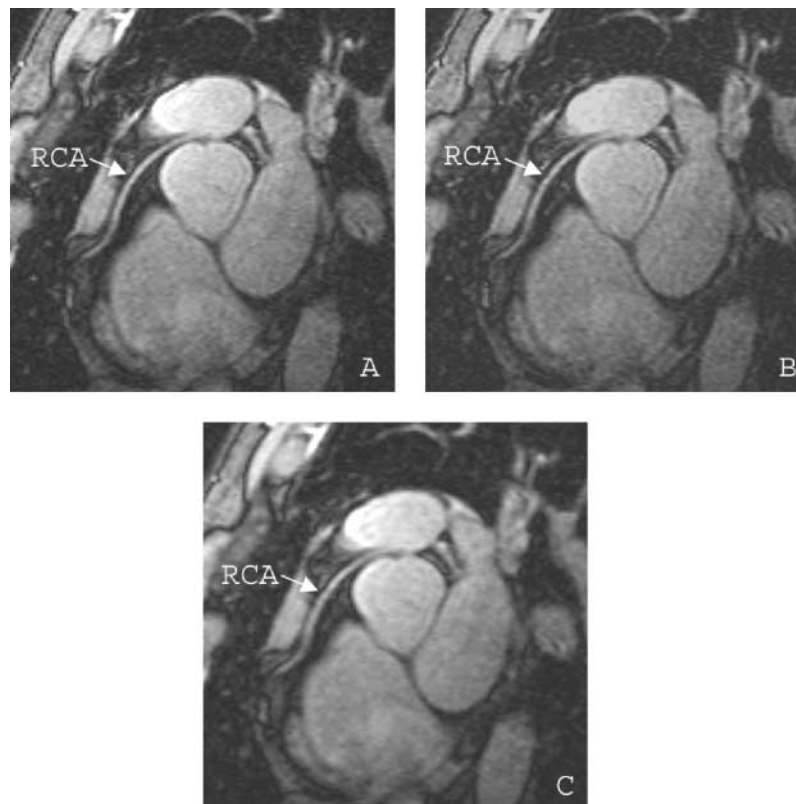
Figure 1.   Images reconstructed from the full k-space data (A), the partial data with PF estimations (B), and the partial data with zero-filling (C). (A) and (B) are of comparable sharpness and are both clearly sharper than (C).

1–5 by two blinded, independent radiologists. Signal to noise ratio (SNR) was compared between the images.

Results: The sharpness measurements of the PF images were comparable to the original images, and significantly better than the ZF images ($p < 0.05$). The mean quantitative measurements were: full k-space, $1.07 \pm 0.13 \, \text{mm}^{-1}$; PF, $1.03 \pm 0.13 \, \text{mm}^{-1}$; ZF, $0.86 \pm 0.13 \, \text{mm}^{-1}$. Qualitative ratings of coronary artery definition in PF images were also significantly better than ZF images ($p < 0.05$), and were comparable to full k-space images. The mean qualitative ratings were: full k-space, reader 1–4.57, reader 2–3.57; PF, reader 1–4.29, reader 2–3.86; ZF, reader 1–2.71, reader 2–2.71. The SNR of the PF images was lower than the full k-space images and the ZF images ($p < 0.05$). The SNR values were: full k-space, 11.5 ± 1.5; PF, 9.7 ± 1.3; ZF, 12.0 ± 1.3. An example of the three reconstructions is shown in Fig. 1.

Conclusions: MR images of the coronary arteries reconstructed from a partial, asymmetric sampling of

k-space with PF estimation of the missing data were significantly sharper than images reconstructed from the same data with zero-filling of the missing data, and were comparable to images reconstructed using full k-space data sets. Although the SNR of the PF images was slightly lower than the full k-space images and the ZF images, it was adequate for clear delineation of the vessel border. The PF images were reconstructed from only 56% of the original k-space data. PF is a potentially useful technique for reducing acquisition time by up to a factor of two or improving resolution for breath-hold coronary MR angiography.

References
1. Xu, Y., et al. *Journal of Magnetic Resonance Imaging*, 14, 628, 2001.
2. Deshpande V.S., et al. *Journal of Magnetic Resonance Imaging*. 13, 676, 2001.

300. Assessment of Inter-site Variability of Morphological Measurements on Carotid Arteries Using Black-Blood MRI

Baocheng Chu, MD,[1] Vasily L. Yarnykh, PhD,[1] John Huston, MD,[2] Dennis L. Parker, PhD,[3] Chun Yuan, PhD.[1] [1]*Radiology, University of Washington, Seattle, WA, USA,* [2]*Radiology, Mayo Clinic and Foundation, Rochester, MN, USA,* [3]*Radiology, University of Utah, Salt Lake City, UT, USA.*

Introduction: Evaluation of morphology of the carotid atherosclerotic plaque is a powerful tool for the control of progression of disease and monitoring of therapy. A generally good reproducibility was demonstrated between morphologic parameters obtained from high-resolution black-blood images of carotid arteries (CA) acquired at a single site with a standardized protocol and highly experienced personnel (1). However, an inter-site reproducibility of carotid imaging has not been studied yet, although this aspect is of critical importance for further application of carotid MRI in multi-center clinical studies.

Purpose: To assess variability of carotid artery morphological measurements using high-resolution black-blood MRI in a multi-center trial setting.

Methods: One healthy volunteer underwent MRI of bilateral CA in three institutions using the identical protocol and phased-array carotid coils on 1.5 T (GE, Signa) scanners operated under 5.8, 8.4, and 9.0 versions of the EPIC software. Two MRI technologists underwent a three-hour training session at the master site (University of Washington) and performed examinations at their sites without supervision. Cross-sectional black-blood images were acquired using a fast spin-echo (FSE) pulse sequence with a quadruple inversion-recovery (QIR) preparation (2), which provides improved quality of blood suppression. The QIR-FSE scan parameters were as follows: TR/TE = 800/10.5 ms, TI1/TI2 = 326/123 ms, echo train = 10, FOV = 16 × 12, slice thickness = 2 mm, Matrix = 256 × 256, NEX = 2, nine slices were acquired. A two-step localization procedure was used to guarantee uniform positioning of a slice pack relative to the bifurcation: 1) the rough position of the bifurcation was found from axial 2D TOF images; 2) the bifurcation was precisely localized using a fast 2D black-blood MR angiography (multi-slice double inversion-recovery technique (3)) in oblique plane aligned through adjacent segments of internal, external, and common CA. One observer evaluated the image quality and performed morphological measurements on each slice using a semi-automated Snake-based algorithm (4). The following parameters were measured bilaterally for common, internal, and external CA: signal-to-noise ratios in the lumen (SNRl) and in the vessel wall (SNRw), lumen area (LA), total vascular area (TVA), and wall area (WA = TVA-LA) Wall volume (WV) was calculated as the sum of WA's on all slices multiplied by the slice thickness. The image specific error (ISE) was defined as the mean absolute difference in the matched images among pairs of institutions. Percentage error (PE) was defined as mean absolute percentage difference among three institutions. Pooled standard deviation (pSD) was calculated across all images and institutions.

Results: The images from all sites demonstrated high quality and efficient blood suppression (Fig. 1). The algorithm for localization of bifurcation resulted in almost identical alignment of slices by all operators (Fig. 1). Results of image analysis are summarized in Table 1.
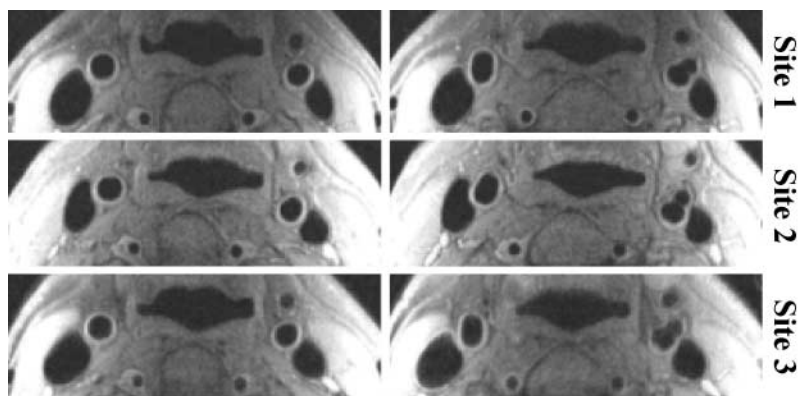
Figure 1. Representative images at two anatomic locations obtained in three institutions.

Table 1. Results of image analysis.

	LA (mm^2)	TVA (mm^2)	WA (mm^2)	WV (mm^3)	SNRl	SNRw
Site 1	29.0	59.7	30.6	550.7	1.2	9.6
Site 2	29.5	61.0	31.5	565.8	1.1	9.4
Site 3	28.7	61.2	32.6	585.9	1.1	9.5
Mean	29.1	60.6	31.6	567.5	1.1	9.5
ISE	1.4	3.3	2.9	—	—	—
PE (%)	2.8	2.1	5.9	—	—	—
PSD (%)	1.3	2.9	2.6	—	—	—

Conclusions: Quantitative measurement of vessel wall morphology is highly reproducible in different institutions with small variation. This study shows the feasibility of application of black-blood carotid MRI for multi-center clinical trials.

References

1. Kang K.J., et al. Magn. Reson. Med. 2000; 44:968–972.

2. Yarnykh V.L., Yuan C. Magn. Reson. Med. 2002; in press.

3. Yarnykh V.L., Yuan C. Proc. ISMRM, 2002; p. 1563.

4. Chao H., et al. IEEE Transactions on Image Processing. 2001; 6:865–873.

301. Multistation Magnetic Resonance Angiography of Lower Limb Ischemic Disease: Correlation with Digital Subtraction Angiography

Adriana S. Matos, MD,[1] Claudio C. de Castro, MD, PhD,[2] Kyiomi K. Uezumi, MD, PhD,[3] Jose V. Kairiyama, MD, PhD,[3] Lucas M. Ferreira, MD,[1] Francisco C. Brochado Neto, MD,[1] Marcelo F. Matielo, MD,[1] Robson B. Miranda, MD,[1] Giovanni G. Cerri, MD, PhD.[4] [1]*Hospital Servidor Publico Estadual, Sao Paulo, Brazil,* [2]*MRI Section, InCor—Heart Institute—University of Sao Paulo, Sao Paulo—SP, Brazil,* [3]*MRI Section, InCor— Heart Institute—University of Sao Paulo, Sao Paulo, Brazil,* [4]*InCor—Heart Institute—University of Sao Paulo, Sao Paulo, Brazil.*

Introduction: Recent studies have shown MR angiography (MRA) as a promising method to study lower limb arterial ischemic disease. However, additional studies are needed to validate MRA as a primary screening method for such patients.

Purpose: To compare digital subtraction angiography (DSA) with tridimensional multistation MRA, performed with single bolus injection of paramagnetic contrast media, in the characterization of lower limb ischemic arterial disease.

Methods: Ten patients with incapacitating claudication or lower limb trophic lesions were prospectively studied by both methods. Each lower limb was divided into 15 arterial segments, and stenosis was evaluated using the following grading scale: grade $0 = 0\,\text{to}\,49\%$, $1 = 50\,\text{to}\,74\%$, $2 = 75\,\text{to}\,99\%$, and $3 = \text{occlusion}$. The most severe lesion of each segment was considered for the study. MRAs were performed in a 1.5 T GE CVMR unit. The exams were scored by two independent observers, blind to disease.

Results: A total of 255 arterial segments were studied, with Kappa of 0.83 (p < 0.001) when comparing both methods. Arterial segments were subdivided in aortoiliac, femoropopliteal and tibiofibular segments, with Kappa of 0.91, 0.85 and 0.77, respectively (p < 0.01).

Conclusions: A high correlation was observed between MRA and DSA in the evaluation of lower limb arterial ischemic disease, which is greater in proximal arterial segments.

302. Nitrate-Induced Coronary Vasodilation by Stress-MRI: A Non-invasive Test of Coronary Vasomotion

Alessia Pepe,[1] Massimo Lombardi,[2] Imola Takacs,[3] Vincenzo Positano,[3] Enrico Hoffmann,[4] Eugenio Picano.[3] [1]*Department of Cardiology, University of*

Palermo, Palermo, Italy, [2]*MRI Laboratory, CNR, Clinical Physiology Institute, Pisa, Italy,* [3]*CNR, Clinical Physiology Institute, Pisa, Italy,* [4]*University of Palermo, Palermo, Italy.*

Introduction: The assessment of coronary response to exogenous nitrovasodilators may have a diagnostic and prognostic impact in patients with coronary artery disease. To date, stress imaging of coronary artery vasomotion has been confined to the catheterization laboratory. Magnetic resonance angiography (MRA) is emerging as a non invasive tool for coronary artery imaging.

Purpose: Aim of this study was to evaluate the feasibility of assessing coronary vasodilation following exogenous nitrates, using MRA.

Methods: Coronary MRA was performed in 10 healthy volunteers (8 male; age 34 ± 11). We used Spiral Spoiled Gradient Echo (SSGE) sequences for imaging of coronary artery lumen. After the baseline short axis view of the coronary artery was obtained, sublingual nitroglycerin (NTG) (0.3 mg) was administered. In all subjects short axis views of the coronary artery were acquired repetitively (8–10 times) from 1 up 10 minutes after NTG administration. Measurements were obtained by two independent investigators.

Results: Interpretable short axis view of left anterior descending artery was obtained in 8 subjects (80%), in the remaining 2 subjects right coronary artery was examined. The inter-observer variability was 15%, the intra-observer variability 4%. The NTG-induced maximal vasodilation was $44 \pm 26\%$. The vasodilator response over time after nitroglycerin was maximal on average at 291 ± 73 seconds, but with substantial heterogeneity.

Conclusions: Entity and time-course of nitrate-induced coronary vasodilation in the left anterior descending and/or right coronary artery can be assessed using MRA with high feasibility and reproducibility. Coronary MRA appears as a suitable candidate for dynamic imaging of coronary vasomotion, as a non-invasive test of coronary smooth muscle cell function.

303. Aorta Root Measurements: Comparison of Echocardiography, 2D Cine MRI, and Contrast-Enhanced 3D MRA

Tim Irwin, BSE,[1] Alan H. Stolpen, MD, PhD,[1] David J. Skorton, MD,[2] Marcia C. Willing, MD, PhD,[3] Thomas D. Scholz, MD,[3] Lizann Bolinger, PhD.[1] [1]*Radiology, University of Iowa, Iowa City, IA, USA,* [2]*Cardiology, University of Iowa, Iowa City, IA, USA,* [3]*Pediatrics, University of Iowa, Iowa City, IA, USA.*

Introduction: Accurate and reproducible serial measurements of the aortic root are essential for managing patients at high risk for developing annuloaortic ectasia (i.e. dilated aortic root) [1]. Although two-dimensional echocardiography (Echo) is currently the gold standard for imaging and measuring the aortic root, the absence of a good acoustic window can preclude complete evaluation. Due to this limitation, other imaging modalities are being explored. The recent development of fast MR scanners with cardiovascular imaging capabilities makes MR an attractive alternative. There are several techniques for obtaining MR images of the aortic root that may be useful for evaluating and following high risk patients.

Purpose: This study set out to address two issues concerning MR-derived measurements of the aortic root. The first was to compare two different MR techniques. The second was to address whether Echo-derived normative data for aortic root dimensions can be applied to MR-derived measurements.

Methods: Between June 1999 and June 2002, 47 patients (age range: 7–70 yrs; mean 32.2 yrs) underwent imaging of the aortic root which included some combination of echocardiography, 2D cine MRI, and gadodiamide-enhanced 3D MRA. All patients had one of the following diagnoses (known or suspected): Marfan syndrome, Ehlers-Danlos syndrome, familial thoracic aortic aneurysm syndrome, aortic coarctation, and biscuspid aortic valve. Of the 47 patients, 41 had both cine MRI and Echo, 27 had both cine MRI and MRA, and 21 had both MRA and Echo.

Cine MRI- and Echo-derived measurements of the aortic root were made at end-diastole in the parasternal long axis view at four locations: (1) annulus (i.e., hinge points of the aortic valve cusps), (2) sinuses of Valsalva, (3) sinotubular junction (i.e., supraaortic ridge), and (4) proximal ascending aorta (Fig. 1). The parasternal long axis view, which is a plane that includes the aortic and mitral valves, proximal ascending aorta, left atrium and left ventricle, was selected visually at the time of imaging. Aortic root dimensions were measured perpendicular to the long axis of the proximal ascending aorta. In contrast, the MRA data set is three-dimensional, and does not require a specific plane to be selected at the time of imaging. MRA data was transferred to an independent workstation, where a plane corresponding to the parasternal long axis was selected automatically by using a custom-designed openGL-based software package. The four aortic root dimensions
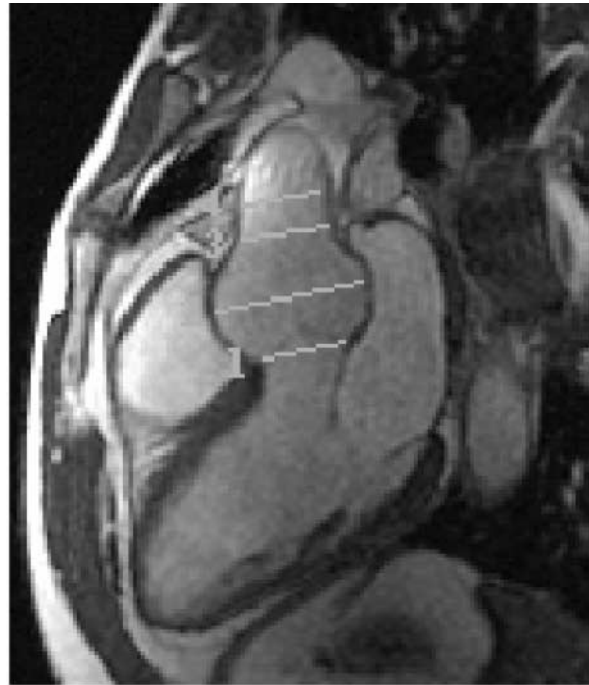
(a)
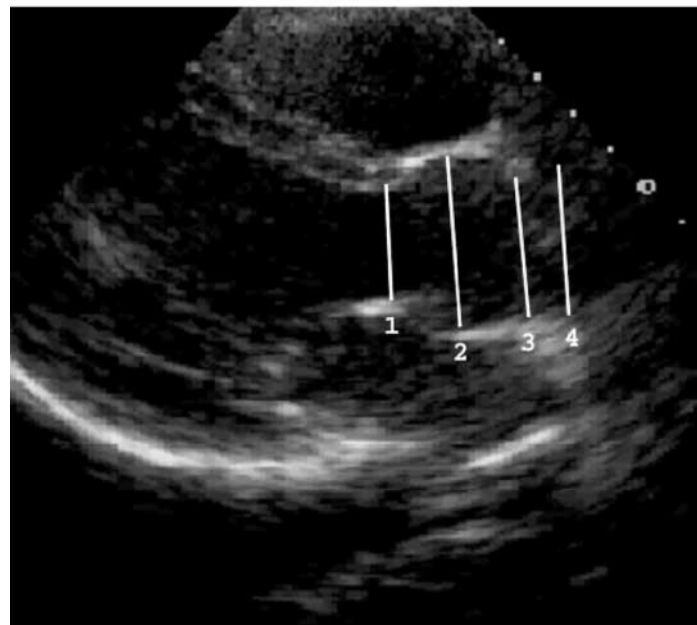
(b)

Figure 1. Parasternal long axis view showing the aortic root and locations of the four measurements in both cine MRI (a) and Echo (b).

were then measured manually on the computer-selected image. At each of the four aortic root locations, pairwise agreement between measurements obtained with the different modalities (Echo, cine MRI and MRA) was determined by plotting the measurements against a line with unit slope. Bland–Altman statistics were used to assess the magnitude and variance of any differences between the techniques (2).

Results: In plots comparing the two MR techniques, the slope was never statistically different from 1 (p > .05) at any of the four aortic root measurements. Comparison of MRA to Echo showed that the slope was statistically different from unity at the annulus and the sinotubular junction. Comparison of cine MRI and Echo showed that the slope was statistically different from unity at the annulus, the sinotubular junction and the ascending aorta. Bland–Altman analysis showed that the mean difference between measurement techniques reached statistical significance only at the sinuses of Valsalva for cine MRI vs. MRA, the annulus and sinotubular junction for MRA vs. Echo, and the sinotubular junction and ascending aorta for cine MRI vs. Echo (Table 1).

Discussion: The data presented in Table 1 show that the correlation between 2D cine MRI and 3D MRA depends on where the measurement is taken. Agreement was good at the sinotubular junction and ascending aorta. However, at the sinuses of Valsalva there was a small, statistically significant, systematic offset in the mean difference of the two measurements. This difference can be explained by the fact that MRA acquisitions are not cardiac-gated and therefore represent a weighted average of systolic and diastolic dimensions. In contrast, cine MRI measurements are made from cardiac-gated images in end diastole. The greater compliance of the aorta at the sinuses of Valsalva could explain why this was the only site to demonstrate a systematic offset. In fact, small changes in the dimension of the sinuses of Valsalva can

be observed in systole and diastole on cine MRI loops. The aortic annulus was also a site of poor agreement between cine MRI and MRA. It is likely that cardiac and aortic valve motion cause significant blurring on non-cardiac-gated MRA images. By comparison, the aortic annulus, the aortic valve hinge points and aortic valve movements are routinely visualized on cine MR images. Consequently, cine MR measurements of the aortic annulus are probably more reliable and reproducible than measurements made from MRA images, and it is to be expected that this location would have the lowest agreement. One strategy for improving the performance of MRA would be to use cardiac gating and force data acquisition to the diastolic phase. This should significantly reduce motion artifact and increase agreement with cine MRI.

The agreement between Echo and either of the MR techniques was not near as good as the agreement between the MR techniques themselves. This could be related to difficulties in making accurate aortic root from Echo images. We suspect that the reproducibility and precision of the Echo measurements is much worse than that of MR, but this needs to be verified experimentally. Because the slopes comparing the MR techniques to Echo differ significantly from 1, the normative aortic root data for Echo may not be valid for either MR technique.

3D MRA has several advantages over cine MRI for measuring aortic root dimensions. Cine MRI requires a technologist to chose, at the time of imaging, the plane from which measurements will be made (similar to Echo).

Table 1. Results of aortic root measurements.

Comparison	Aortic Site	n*	R^2	Slope	Mean diff (cm)	Std dev of diff (cm)
MRA/MRI	Annulus	26	0.39	0.71	−0.03	0.30
	Sinuses	27	0.80	0.88	0.14**	0.29
	ST Junction	27	0.90	1.01	−0.06	0.18
	Asc Aorta	27	0.86	0.91	0.02	0.26
MRA/Echo	Annulus	18	0.21	0.21***	0.16	0.43
	Sinuses	21	0.68	0.76	0.23**	0.34
	ST Junction	19	0.47	0.48***	−0.27**	0.51
	Asc Aorta	14	0.66	0.84	−0.09	0.37
MRI/Echo	Annulus	38	0.22	0.43***	0.10	0.39
	Sinuses	40	0.83	0.93	0.04	0.33
	ST Junction	37	0.61	0.65***	−0.34**	0.50
	Asc Aorta	29	0.65	0.66***	−0.23**	0.42

*n is the number of measurements in the comparison. Measurements were not always available at all four locations on the echo data. In one MRI study, the presence of a prosthetic aortic valve precluded the measurement at the annulus.
**Statistically significant (p < .05).
***Statistically different from 1 (p < .05).

3D MRA uses a volumetric data set, so the parasternal long axis plane can be selected at a later time by an expert. Using 3D MRA data, it should be possible to accurately and automatically define and measure cross sectional areas and volumes of the aortic root. Such measurements may provide more prognostic information than simple one-dimensional measurements from Echo or cine MRI.

References

1. Roman M.J., Devereux R.B., Kramer-Fox R., O'Loughlin J. Two-Dimensional Echocardiographic Aortic Root Dimensions in Normal Children and Adults. Am. J. Cardiol. 64:507–512, 1989.

2. Bland J., Altman D. Statistical methods for assessing agreement between two methods of clinical measurements. Lancet 1:307–310, 1986.

304. Endothelial Function Assessed by Cardiovascular Magnetic Resonance Is Reduced in Thalassemia Major

Morten B. Sorensen, MB, BS, PhD,[1] Mark Westwood, MB, BS, MRCP,[1] Lisa Anderson, MB, BS, MRCP,[1] Peter Gatehouse, PhD,[1] Beatrix Wonke, MD, FRCP,[2] Dudley J. Pennell, MD, FRCP.[1] [1]*CMR Unit, Royal Brompton Hospital, London, United Kingdom,* [2]*Haematology, Whittington Hospital, London, United Kingdom.*

Introduction: Increased iron deposition is regarded as a risk factor for advanced atherosclerosis and coronary artery disease. Thalassemia Major (TM) represents the purest human model for iron overload. Essential transfusions from infancy result in massive iron overload, which affects the cardiovascular system. Iron overload in TM might be linked to endothelial dysfunction and excess atheroma formation.

Purpose: To assess endothelium-dependent arterial reactivity in young men with TM.

Methods: Flow mediated (FMD) and nitrate induced (GTN) change in brachial artery cross sectional area were measured by True FISP cardiovascular magnetic resonance (CMR) to assess endothelium dependent and independent arterial reactivity. We have developed and validated this new technique in a recent publication (Circulation 2002; 106: 1646–51) and have shown it to be accurate for assessment of rapid change in arterial tone. 10 men with TM (age 30.5 ± 7 years) and 10 healthy male controls (age 30.4 ± 4 years) were studied.

Results: Endothelium dependent arterial reactivity was significantly reduced in men with TM compared to healthy controls (1.6 ± 3% vs. 6.3 ± 8%, $p < 0.05$). No difference was detected in endothelium independent arterial reactivity (42.1 ± 16% vs. 35.9 ± 12%, $p = 0.19$).

Conclusions: Accurate measurements of endothelium dependent arterial responses by CMR are significantly reduced in patients with TM. The proposed relationship between iron overload and endothelial dysfunction in TM detail a new mechanism for cardiovascular morbidity in this common genetic disorder. Excess atheroma formation in TM is of importance with improving therapy and increasing longevity.

305. Magnetic Resonance in Pulmonary Arterial Hypertension: A Non-invasive Alternative in the Assessment of Right Ventricular Function

Teresa M. Caralt, MD,[1] Jaime Morales-Blanhir, MD,[2] Juan A. Barberá, MD,[2] Juan R. Ayuso, MD,[1] Carmen Ayuso, MD,[1] Marcelo Sanchez, MD,[1] Mario Pagés, MD,[1] Ramon Zuñiga, MD.[1] [1]*Radiology, Hospital Clinic, Barcelona, Spain,* [2]*Pulmonary Medicine, Hospital Clinic, Barcelona, Spain.*

Introduction: Magnetic resonance (MR) is a nonivasive technique that provides anatomic and functional information of right ventricle (RV) and pulmonary artery.

Purpose: The study was aimed to investigate the potential clinical applicability of MR in assessing RV function in patients with pulmonary arterial hypertension (PAH).

Methods: We studied prospectively 14 patients (41 ± 4 yr; 8w/6m) with PAH using right heart catheterization (RH cath) and MR. We measured with MR: stroke volume (SV), cardiac output (CO), right ventricular hypertrophy index (RVHI) and pulmonary artery distensibility (PAD).

Results: At RHcath mean pulmonary artery pressure (PAP) was 44 ± 3 mmHg; CO (thermodilution), 3.84 ± 0.36 l/min; SV 54 ± 6 ml.;and pulmonary vascular resistance, 889 ± 105 dyn. seg^{-1} cm^{-5}. Using MR, mean CO was 3.78 ± 0.35 l/min and it correlated with that measured by RHcath (r = 0.89, $p < 0.01$). Mean SV measured by MR was 55 ± 6 ml and it also correlated with RHcath SV (r = 0.89, $p < 0.01$). RVHI was increased in 64% of patients (mean, 0.70 ± 0.37; normal, < 0.5), whereas PAD was slightly decreased (mean 8.8 ± 1.6%; normal 13–30%).

Conclusions: We concluded that MR provides an accurate assessment of RV function in patients with PAH

and that it might be useful in the follow-up of patients, avoiding the necessity to repeat right heart catheterization.

306. Combined Transesophageal and Surface MRI Show Precisely the Statin-Induced Reduction in Aortic Atherosclerotic Plaque Volume in Patients with Documented Cardiovascular Disease

Henning Steen. *Cardiac MRI, Johns Hopkins Hospital, Baltimore, MD, USA.*

Introduction: MRI is a highly precise method for vessel wall and plaque imaging and their changes. Previous lipid lowering trials have shown minimal decrease in vessel luminal stenosis in the face of significant reduction in adverse clinical outcomes. These results have been interpreted as suggesting that the effects of statins on atherosclerosis are mediated by non-lipid lowering effects.

Purpose: We hypothesized that combined transesophageal and surface MRI can precisely show changes in plaque size in conjunction with concomitant alterations in serum lipid

Methods: Atherosclerotic plaque volume in the thoracic aorta was measured by combined surface and transesophageal MRI (TEMRI) in patients with known cardiovascular disease. As part of an ongoing clinical trial, patients were randomized to treatment with simvastatin 20 or 80 mg daily and followed with serial lipid panels and with TEMRI. We previously established a standard error of 2,24 % – 2,65 % for TEMRI measurement of aortic plaque volume. Therefore, any difference in plaque volume over time of less than double the standard error should not be considered significant.

Results: Atherosclerotic plaque volume in the thoracic aorta was measured by combined surface and transesophageal MRI (TEMRI) in patients with known cardiovascular disease. As part of an ongoing clinical trial, patients were randomized to treatment with simvastatin 20 or 80 mg daily and followed with serial lipid panels and with TEMRI. We previously established a standard error of 2,24 % – 2,65 % for TEMRI measurement of aortic plaque volume. Therefore, any difference in plaque volume over time of less than double the standard error should not be considered significant.

Conclusions: TEMRI is a precise method of monitoring alterations in aortic plaque burden. Pharmaceutical effects of plaque size reduction according to the mechanisms of statin-induced plaque

regression can be monitored in patients with documented cardiovascular disease very precisely.

307. Image Quality Assessment of Coronary MRA

Martijn S. Dirksen, Hildo J. Lamb, PhD, Rob J. van der Geest, MSc, Albert de Roos, MD. *Radiology, Leiden University Medical Center, Leiden, Netherlands.*

Introduction: Coronary MRA is a promising technique for non-invasive evaluation of coronary artery disease. Various technical modifications are currently under investigation to improve the diagnostic accuracy of coronary MRA, such as parallel imaging, steady-state free precession, spiral data acquisition and the development of blood pool contrast media. Objective measures are needed to asses the contribution of those techniques as compared to conventional techniques. A universally applicable method for evaluation of image quality of coronary MRA using 4 image-parameters has not been described previously.

Purpose: To evaluate a method to quantitatively assess the image quality of coronary MRA based on the calculation of contrast-to-noise, signal-to-noise, vessel length and vessel-edge sharpness, using standard available equipment.

Methods: The proposed method was tested in a pig model (n = 7). Two acquisitions were compared using the parameters for contrast-to-noise, signal-to-noise, vessel length and vessel-edge sharpness. Acquisition 1 consisted of 3D gradient echo coronary MRA without exogenous contrast enhancement. Acquisition 2 was similar to acquisition 1, but was performed in conjunction with a blood pool contrast agent (Vistarem®; Guerbet, France). For the contrast-to-noise and signal-to-noise calculations, regions-of-interest were drawn on the coronary arteries and perivascular tissues. The vessel-length was determined using curvilinear multi-planar reconstruction. Vessel-edge sharpness was based on the automated calculation of a set of line intensity profiles across the coronary arteries (see Fig. 1). Comparison of the image-parameters for both acquisitions was performed using student-t testing. Correlation analysis was performed to illustrate the attributive effect of each individual parameter to the overall assessment of image quality.

Results: A method for quantitative image assessment is described. Using this method, two different acquisitions could be distinguished based on measurements for contrast-to-noise (6.2 ± 0.8 vs. 8.2 ± 0.9; p = 0.0080),
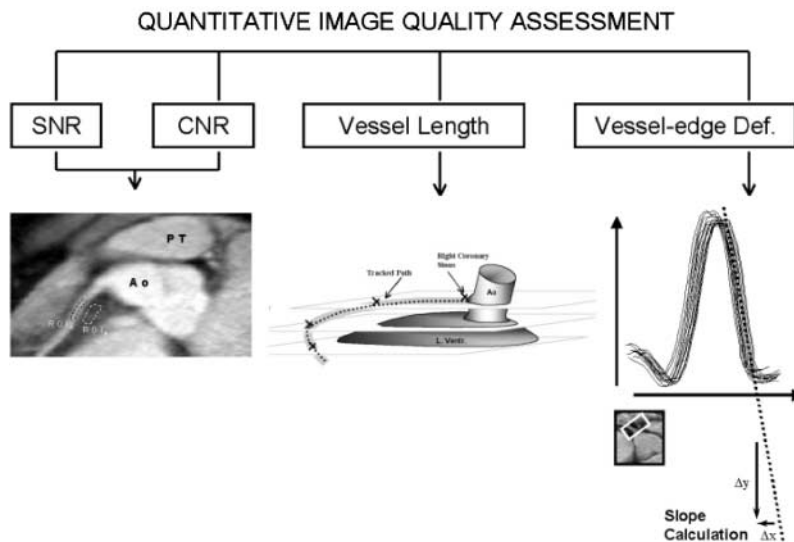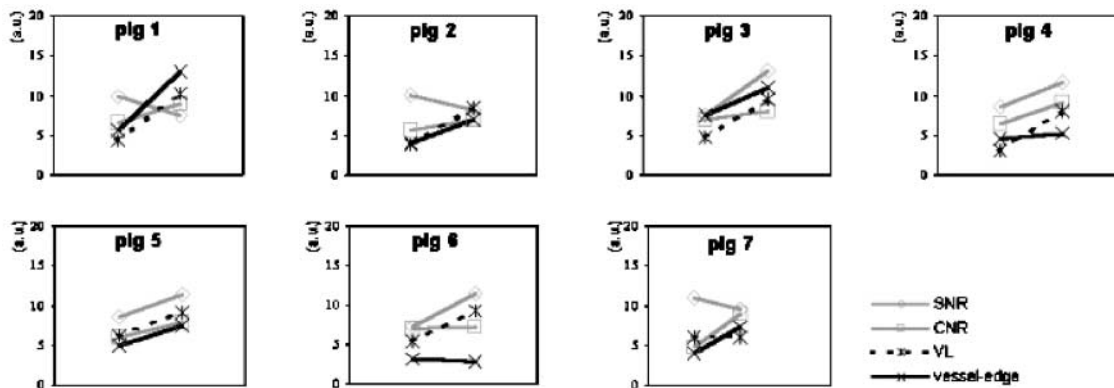
Figure 1.

Figure 2. Graphic representation of the correlation between the image parameters. The four image parameters (before and after administration of the contrast agent) are plotted for each animal. It is shown that there is low correlation between the parameters, which supports the simultaneous determination of all four parameters for a complete coronary image quality assessment.

signal-to-noise (9.0 ± 1.4 vs. 10.4 ± 2.1; $p = 0.29$), vessel-length visualization (48.2 ± 11.6mm vs. 86.5 ± 13.8mm; $p = 0.0020$) and vessel-edge sharpness (4.9 ± 1.5 vs. 7.7 ± 3.4; $p = 0.022$) (acquisitions without exogenous contrast versus acquisitions with a blood pool agent). Correlation analysis shows that each parameter has specific utility in the overall assessment of image quality (see Fig. 2).

Conclusions: The combined application of contrast-to-noise measurements, signal-to-noise measurements, vessel-length determination and calculation of vessel-edge sharpness allows for objective evaluation of the image quality different coronary MRA techniques.

308. Improved Coronary MRA with a Rapid Clearance Blood Pool Agent: Initial Human Results

Martijn S. Dirksen, MD,[1] Hildo J. Lamb, PhD,[1] Harrie C.M. van den Bosch, MD,[2] Catinka Peels, MD,[3] Albert de Roos, MD.[1] [1]*Radiology, Leiden University Medical Center, Leiden, Netherlands,* [2]*Radiology, Catharina Ziekenhuis Eindhoven, Eindhoven, Netherlands,* [3]*Cardiology, Catharina Ziekenhuis Eindhoven, Eindhoven, Netherlands.*

Introduction: Recent pharmaceutical developments have resulted in the design of a blood pool contrast agent with rapid clearance properties for coronary MRA (Vistarem®; Guerbet, France). Conventional blood pool agents

Table 1.

	Without Vistarem	With Vistarem
Contrast-to-noise ratio (mean $\pm$ SD)	9.4 $\pm$ 0.8	16.3*
Signal-to-noise ratio (mean $\pm$ SD)	14.3 $\pm$ 1.4	19.4*

*Improved as compared to coronary MRA without contrast agent ($>$3 times SD).

have shown useful for improving coronary MRA due to their selective intravascular distribution. A rapid clearance blood pool agent combines selective intravascular distribution with rapid renal elimination. The rapid elimination allows for repeat injections, thereby permitting combined acquisition schemes such as coronary MRA with rest-stress myocardial perfusion imaging.

Purpose: To evaluate Vistarem as feasible contrast medium for coronary MRA in humans.

Methods: Five patients were included in this preliminary study. Vistarem is a monodisperse, monogadolinated macrocyclic blood pool agent. The molecular weight is 6.47kDa, which is too high for capillary extravasation, but low enough to freely pass the glomerular fenestration of the kidneys. Four patients (mean age 58.6 $\pm$ 12.4) underwent coronary MRA of the left coronary artery using a non-contrast enhanced T2 preparation technique, whereas one patient (age 62) underwent coronary MRA using Vistarem. The acquisition technique was based on a 3D gradient recalled echo sequence combined with respiratory navigator gating. Fat saturation and a 90° prepulse were applied for suppression of background signal. Imaging was performed on a Philips Gyroscan 1.5T system equipped with powertrak 6000 gradients and all 5 elements of a cardiac synergy surface coil (Philips Medical Systems, Best, Netherlands). Image evaluated was based on calculation of contrast-to-noise ratio and signal-to-noise ratio.

Results: The images that were acquired in combination with the rapid clearance blood pool agent showed improved image quality as compared to the acquisitions without contrast material ($>$3 times SD) (see Table 1).

Conclusions: Vistarem has potential as a contrast medium for coronary MRA. The results of the present study warrant further clinical investigation.

309. Endothelial Function Is Impaired in Women with Polycystic Ovary Syndrome

Morten B. Sorensen, MB, BS, PhD,[1] Carole Robertson, RN,[2] Stephen Franks, MD, FRCP,[2] Dudley J. Pennell, MD, FRCP,[1] Peter Collins, MD, FRCP.[3] [1]*CMR Unit, Royal Brompton Hospital, London, United Kingdom,* [2]*Department of Reproductive Science & Medicine, Imperial College School of Medicine, London, United Kingdom,* [3]*Cardiac Medicine, Imperial College School of Medicine, London, United Kingdom.*

Introduction: Polycystic ovary syndrome (PCOS) is associated with atherogenic metabolic abnormalities and has been linked to coronary atheroma formation. However data are inconsistent both with regard to cardiac morbidity but also with regard to endothelial function in women with PCOS. Intrinsic estrogen levels, which often are high in PCOS, could be a protective factor.

Purpose: To assess arterial function and estradiol levels in women with PCOS and in healthy controls with a regular menstrual cycle.

Methods: Endothelium-dependent (flow-mediated dilatation—FMD) and -independent (glyceryl trinitrate—GTN) changes in brachial artery area were measured by cardiovascular magnetic resonance in 14 women with PCOS and irregular menstrual cycles (mean age 33 $\pm$ 4 years) and in 11 controls with regular menstrual cycle (mean age 31 $\pm$ 6 years). Arterial function was assessed twice in both women with PCOS (during menses and 14 days later) and controls (during menses and at calculated day of subsequent ovulation). Estradiol levels were measured by RIA at each visit.

Results: FMD was greatly reduced in women with PCOS compared to controls both during the menstrual phase (-1.4% vs 8.0%, p $<$ 0.01) and at mid-cycle (2.5% vs 12.5%, p $<$ 0.01) without differences in GTN responses. Between visits, significant differences were observed in estradiol levels in controls (79pM vs. 624pM, p $<$ 0.01) but not in women with PCOS (117pM vs. 236pM, NS). Total cholesterol was not different between women with PCOS and controls (4.9mM and 5.1mM, NS).

Conclusions: PCOS is linked to reduced endothelial function, which might transform into increased cardiovascular risk in later life. Lack of cyclical changes in circulating estrogen with PCOS might be linked to adverse effects on the endothelium.

310. Various Adventitial Enhancement Patterns Are Quantified by CE MRI of Carotid Artery

Annette U. Kampschulte,[1] Williams S. Kerwin,[2] Thomas S. Hatsukami,[2] Chun Yuan.[2] [1]*Radiology,*

University of Washington, Seattle, WA, USA,
[2]*Univeristy of Washington, Seattle, WA, USA.*

Introduction: Contrast enhancement (CE) in the outer wall of atherosclerotic arteries is hypothesized to be associated with neovascularisation entering the plaque from the adventitia and may be a sign of plaque vulnerability.

Purpose: The purpose of this study was to investigate the MRI pattern of adventitial CE by measuring the percent enhancement of both sides in carotid endarterectomy (CEA) patients.

Methods: Non contrast enhanced and contrast enhanced (Omniscan) carotid artery images from 17 patients scheduled for CEA were used to quantify the enhancement of the outer wall boundary. One radiologist measured the average intensity of the left and right carotid artery outer rims on matched pre and post-contrast T1 weighted double inversion recovery images (TR/TI/TE = 800/220/9.3 msec, slice thickness 2 mm). Axial cross sections of the common carotid artery (CCA), bifurcation (Bif), and internal carotid artery (ICA) were analyzed and the percent change of the adventitial CE was calculated for each.

Results: The average percent enhancement (PE) for all patients and sides was 61.7% ± 20.8%. There was an apparent association of enhancement with the lesion type (advanced complicate vs. necrotic vs. fibrotic). Variations of the PE have been seen at different locations, in particular minor peaks were observed in the proximal CCA and distal ICA.

Conclusions: Quantitative measurement provides a tool to evaluate contrast enhanced MRI and assess the pattern of adventitial CE. Variations of PE at different locations and different lesion types are observed. Evaluation of such enhancement pattern may be important to understand the association of the vasa vasorum and neovasculature in atherosclerotic plaque progression.

311. Inter-study Reproducibility of Volume Selective 3D Turbo Spin Echo Technique for Quantifying Total Carotid Artery Vessel Wall Volume

Anitha Varghese, Lindsey A. Crowe, Raad H. Mohiaddin, Peter D. Gatehouse, Guang Zhong Yang, David N. Firmin, Dudley J. Pennell. *Royal Brompton Hospital, London, United Kingdom.*

Introduction: CMR has been validated for the assessment and monitoring of carotid artery and aortic athero-sclerotic plaque burden.
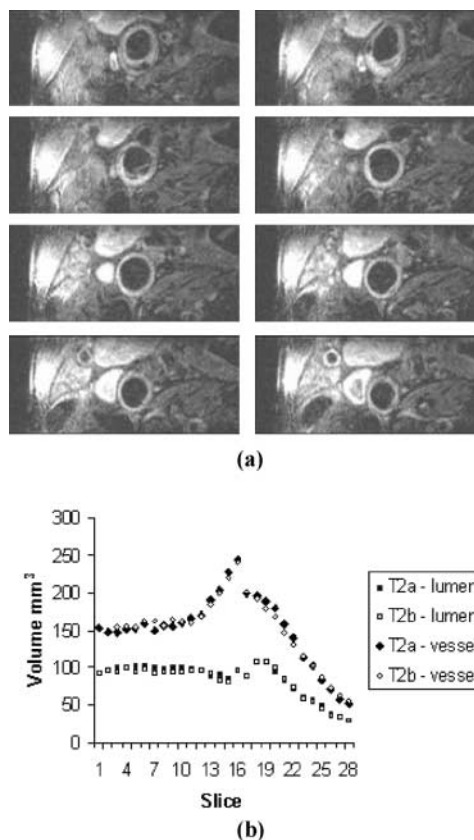
Figure 1. (a) Example of a Slices from T1-weighted TSE Scan. (b) Inter-study reproducibility of lumen and total vessel volume for patient above.

Purpose: To develop a volume selective 3D Turbo Spin Echo (TSE) sequence for arterial wall imaging and evaluate inter-study reproducibility in patients.

Methods: Inter-study reproducibility was evaluated in 7 patients with evidence of carotid artery disease by carotid ultrasonography using a Siemens Sonata scanner and a purpose-built carotid coil. Each scan took 30 minutes and was performed twice with a minimum inter-scan time of one hour. Typical sequence acquisition order and typical parameters were as follows: 2D multi-slice time-of-flight (TOF); *T1-weighted 3D volume-selective TSE* (matrix size = 256, 0.47 × 0.47mm pixels; 28 slices of 2mm thickness; field-of-view 120 × 24mm; TE 11ms; TR depending on patient's heart rate; echo train length 11); and *T2-weighted 3D volume-selective TSE* (matrix size 256, 0.47 × 0.47mm pixels; 28 slices of 2mm thickness; TE 53ms; TR depending on patient's heart rate; echo train length 11). The 56mm region centered around the carotid bifurcation was assessed and

analyzed by a single observer using in-house software (CMRtools, ©Imperial College) following randomization and anonymisation by a second observer. Data was collected in the form of cross-sectional CMR images from which total vessel wall volume was calculated by subtraction of total lumen volume from total vessel wall volume (Fig. 1a and b).

Results: The total vessel wall volume for scans 1 and 2 was $1.38cm^3$ and $1.47cm^3$ and were not significantly different from each other (mean difference $0.090cm^3$, $P = 0.11$). The standard deviation of the differences between the 2 measurements was $0.13cm^3$ yielding a coefficient of variation of 9.0%.

Conclusion: Volumetric analysis of carotid artery plaque using 3D volume selective CMR is efficient and reproducible in comparison with 2D techniques. Using this technique, power calculation indicates that a sample size of 16 would enable a difference over time in plaque volume of $0.13cm^3$ to be detected (80% power).